remote sensing

MDPI

Communication

Terrestrial and Martian Paleo-Hydrologic Environment Systematic Comparison with ASI PRISMA and NASA CRISM Hyperspectral Instruments

Angelo Zinzi [1,2,*], Paola Manzari [1,2], Veronica Camplone [2,3,4], Eleonora Ammannito [1], Giuseppe Sindoni [1], Francesco Zucca [4] and Gianluca Polenta [1,2]

[1] Agenzia Spaziale Italiana (ASI), Via del Politecnico snc, 00133 Rome, Italy; paola.manzari@asi.it (P.M.); eleonora.ammannito@asi.it (E.A.); giuseppe.sindoni@asi.it (G.S.); gianluca.polenta@asi.it (G.P.)
[2] ASI Space Science Data Center (ASI-SSDC), Via del Politecnico snc, 00133 Rome, Italy; veronica.camplone@ssdc.asi.it
[3] INAF Osservatorio Astronomico di Roma (INAF-OAR), Via Frascati, 33, 00078 Monte Porzio Catone, RM, Italy
[4] Earth & Environmental Sciences Department, University of Pavia, Via Adolfo Ferrata, 7, 27100 Pavia, PV, Italy; francesco.zucca@unipv.it
* Correspondence: angelo.zinzi@asi.it

Abstract: The comparative analysis of hyperspectral data from different instruments can provide detailed information on the composition and geology of similar environments on different planets. This study aims to compare data acquired from the PRISMA satellite, used for Earth observation, with those collected by the CRISM spectrometer onboard the Mars Reconnaissance Orbiter, orbiting Mars, in order to analyze the geological and mineralogical differences between the morphologies present on the two planets of interest. The comparison of these data will allow us to examine the mineralogical composition, highlighting the similarities and differences between the terrestrial and Martian environments. In particular, in this study, we present a method to refine the interpretation of spectral features of minerals commonly found in paleo-hydrological environments on Mars and identified also by field analysis of similar terrestrial sites, thus allowing us to improve the Martian sites' characterization. Thanks to this approach, we have been able to find spectral similarities (e.g., band positions, band ratios) among specific Earth and Mars sites, thus demonstrating that it could be further expanded, by systematically using Earth-observation orbiting instruments to better characterize and constrain Martian spectral data.

Keywords: Mars; Earth; hyperspectral; mineralogy; comparison

check for updates

Academic Editors: Jose Moreno and Jonathan H. Jiang

Received: 30 October 2024
Revised: 12 February 2025
Accepted: 20 February 2025
Published: 22 February 2025

Citation: Zinzi, A.; Manzari, P.; Camplone, V.; Ammannito, E.; Sindoni, G.; Zucca, F.; Polenta, G. Terrestrial and Martian Paleo-Hydrologic Environment Systematic Comparison with ASI PRISMA and NASA CRISM Hyperspectral Instruments. *Remote Sens.* **2025**, *17*, 758. https://doi.org/10.3390/rs17050758

Copyright: © 2025 by the authors. Licensee MDPI, Basel, Switzerland. This article is an open access article distributed under the terms and conditions of the Creative Commons Attribution (CC BY) license (https://creativecommons.org/licenses/by/4.0/).

1. Introduction

Since the first images of the Martian surface sent back to Earth by NASA's Mariner 4 camera, it has been evident that several structures observed might have been shaped by flowing water.

With the stream of missions sent to Mars in the following decades, the evidence supporting the presence of water became increasingly convincing.

By the 1990s, NASA's approach to Martian exploration had begun to recognize the "follow the water" strategy [1]. All these missions were indeed developed in order to allow a more accurate characterization of the surface geology, with the aim of revealing and understanding the connections with ancient water routes, valleys, and basins of the planet (e.g., [2]).

Apart from high-resolution imagers, allowing the detection of geomorphological clues of signatures of flowing water, a major kind of instrumentation able to accomplish this aim is that which inspects InfraRed (IR) spectra at wavelengths where evaporitic and sedimentary minerals exhibit their characteristic spectral signature, mostly due to the OH bond.

As technology has advanced, these IR instruments have made a significant leap in quality, passing from spectrometers without spatial resolution capabilities [3] and multi-filter imagers [4] to advanced hyperspectral devices, capable of achieving resolution of a few meters on the Martian surface.

Among these, CRISM (Compact Reconnaissance Imaging Spectrometer for Mars) on board NASA's Mars Reconnaissance Orbiter (MRO) [5] stood out for its ability to operate in the long term, managing to provide a detailed mapping of the signs of ancient water acting in several craters, thanks to unprecedented resolution, both spatial and spectral. Since these paleo-hydrological environments on Mars will continue to be a focal point for scientific research and exploration, not only for outlining the chronology of the Martian landscape, but also for their potential implications for astrobiology (e.g., [6]), it becomes essential to increase the level of precision in identifying structure, ensuring detailed resolution at a fine scale.

It is, therefore, clear how IR spectral observation by remote-sensing instruments can be considered crucial in providing an accurate view of planetary surfaces, even unveiling major details about the history of the planetary surfaces. However, a distinctive aspect of Earth geomorphological studies compared to Mars involves the integration of satellite data with in situ investigations. On Earth, satellite observations are regularly enriched and verified through direct field studies, allowing for a deeper and more accurate understanding of the observed phenomena. In contrast, on Mars, this synergy is limited to areas explored by Martian rovers, which cover only a very small fraction of the planet's surface. This difference highlights the unique challenges of Martian exploration, where the ability to conduct in situ investigations is significantly reduced, making the interpretation of satellite data more complex and, in some cases, less immediate.

A possible solution to this issue may be represented by the comparison of hyperspectral data acquired over terrestrial areas with geologic histories similar to those of the paleo-hydrological zones of interest on Mars with field analysis, able to reach a level of detail that can be the only way to discriminate among a series of different hypotheses driven by remote-sensing analysis.

In response to this challenge, in this study, we have adopted an innovative approach, opting for a direct comparison between the spectral data acquired by CRISM on Mars and those obtained for the Earth by the PRISMA (PRecursore IperSpettrale della Missione Applicativa—Hyperspectral Precursor of the Application Mission) satellite, a mission of ASI (Agenzia Spaziale Italiana—Italian Space Agency) in Earth orbit since 2019. These instruments share similar spatial and spectral resolutions, making this comparison particularly promising. By carefully selecting a series of areas on Earth that feature geomorphologically and spectrally similar environments to the Martian paleo-hydrological zones of interest, we can conduct a comparison between the geology of Mars and that of Earth. This method allows us to use Earth as a laboratory for the "ground truth", providing valuable reference points to calibrate and interpret our analysis of Martian data, with the aim of deepening our understanding of the ancient fluvial dynamics and wet weathering [7] of the Red Planet.

This work is structured as follows: Section 2 describes the two datasets used (PRISMA and CRISM), the process of selecting areas of interest on Earth and the reduction in PRISMA data; Section 3 presents the analysis of PRISMA data in the zones of interest; Section 4

conducts a comparison with the Martian results of CRISM; and Section 5 is dedicated to conclusions and future perspectives.

2. Materials and Methods

2.1. PRISMA

ASI PRISMA was launched on 22 March 2019, using a VEGA launcher, which placed it in a sun-synchronous orbit at an altitude of 615 km, with an inclination of 98° and a Local Time on Descending Node set at 10:30.

PRISMA [8] is equipped with two different payloads: (1) a panchromatic one, optimized over the entire visible spectral range (0.4–0.7 μm), reaching a spatial resolution of 5 m/pixel, and (2) a hyperspectral one with 240 total bands from 400 to 2505 nm at 14 nm of spectral resolution and a nominal spatial resolution of 30 m/pixel.

The hyperspectral component of PRISMA is further divided into two different channels, partially overlapping: (a) VNIR, with 66 bands between 400 and 1010 nm, and (b) SWIR, with 174 bands ranging from 920 to 2505 nm.

All the PRISMA observations are available in HDF5 format upon registration at the official portal (https://prisma.asi.it—accessed on 19 February 2025) and can also be requested directly by the authenticated users.

PRISMA hyperspectral data are categorized as follows:

- L1: Top-of-atmosphere spectral radiance.
- L2B: At-surface radiance
- L2C: At-surface reflectance
- L2D: At-surface geocoded reflectance

For this study we mainly used the L2D data, already corrected for both atmospheric effects and geometric distortions.

2.2. CRISM

CRISM [5], the hyperspectral detector onboard the NASA's MRO mission, was launched on 12 August 2005, and has been orbiting Mars since 10 March 2006. It operates in a sun-synchronous orbit with altitudes ranging between 250 and 316 km, an inclination of 93°, and the Local Time of the Descending Node set at 03:00.

CRISM covers a spectral range between 362 and 3920 nm, with a spectral sampling of 6.55 nm/channel and a spatial resolution of 18.4 m/pixel at 300 km altitude.

CRISM data are differentiated on the basis of their spatial resolution into the following categories:

- Targeted Mode (Full-Resolution Targeted—FRT), with high spectral (545–655 channels) and spatial resolution (~18–36 m/pixel), used for detailed mineralogical studies.
- Half-Resolution Targeted (HRL) and Half-Resolution Short (HRS), with lower spatial resolution (~36–72 m/pixel) but still with high spectral detail, used when full resolution is not needed.
- Along-Track Summing (ATS), used to reduce data volume by averaging pixels in the along-track direction, used for specific targets where high spatial resolution is unnecessary.
- Mapping Mode (MSP—Multispectral Survey Mode): lower spectral resolution (~72 selected channels) but covering large areas, used for broad mineralogical mapping.
- Emplacement (EPF—Emission Phase Function Mode), which acquires multiple views of a target at different angles, helping study surface photometric properties and atmospheric effects.

In this work, we used both FRT and HRL CRISM data.

2.3. Selection of the Studied Regions

To achieve the goal of this study, we recognized the need to select regions on Earth that exhibit geomorphological characteristics similar to those observed on interesting sites on Mars, such as Jezero crater (e.g., [9,10]). This Martian crater, with a diameter of approximately 49 km, and located to the northwest of the Isidis impact basin on Mars, displays unique features suggesting a history rich in fluvial activity [11].

In particular, Jezero has two ancient river deltas, indicating that the crater once hosted a lake, fed by rivers that transported sediments into the basin [12]. The two fan deposits identified in the Jezero crater have different mineralogical compositions, according to studies based on CRISM hyperspectral reflectance data published by [13]. The deposit of the northern cone, which shows a high degree of erosion, is characterized by a spectral signature that indicates the presence of a combination of olivine and carbonate, both hydrated and anhydrous, rich in magnesium, and further enriched by hydrated minerals such as Fe/Mg smectites. On the other hand, the deposit of the western fan, better preserved, reveals a predominance of Fe/Mg smectite, such as nontronite or saponite, with more sporadic occurrences of magnesium-rich carbonate and olivine [13].

This rich knowledge base allows for direct and important comparisons with data collected by NASA's MRO mission on Mars, particularly through the spectral analysis performed by the CRISM instrument.

The integration of Martian observations with similar terrestrial data, in comparable geomorphological contexts, opens the way to new interpretations and a deeper understanding of the geological processes that have influenced and continue to influence the surface of both planets. Through this study, the aim is not only to explore Martian geological dynamics but also to enrich our understanding of Earth, further highlighting the importance of space missions in contributing to geological science in general.

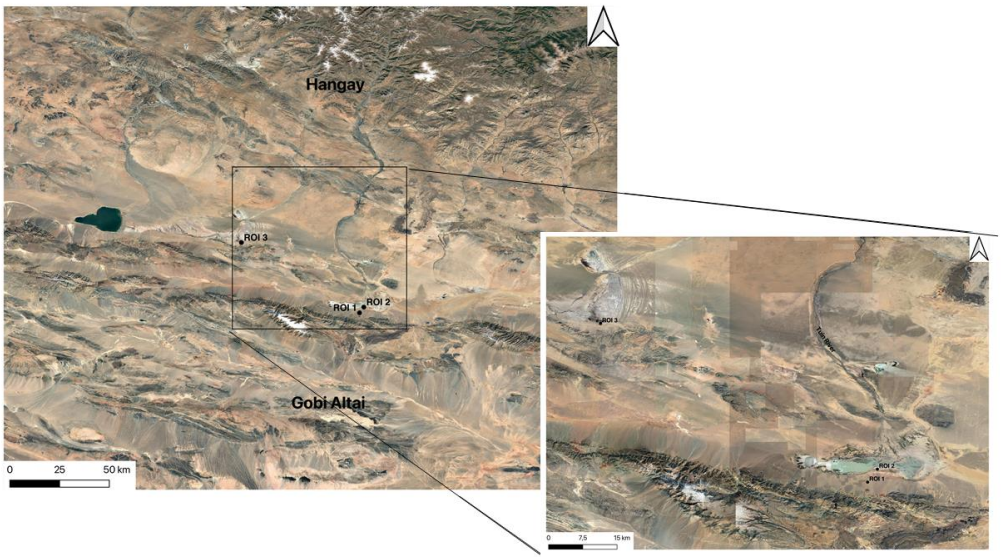
The conditions we are looking for, such as aridity, vast desert areas, the presence of paleo-deltas, and deltaic deposits, are found in some parts of our planet. However, our selection of study areas was not based only on these visual or geomorphological similarities. A crucial factor was the existence of field analyses that could provide a precise description of the site's mineralogy, a key element for accuracy and comparative analysis.

We therefore focused our attention to two different terrestrial sites, Gobi Lakes and Dalinouer area (Table 1), located in desertic or semi-desertic regions and exhibiting distinctive morphological features, such as multiple terminal fans [14] and lobate deltas or paleo-deltas somewhat similar to those found on Mars. We searched for both geological similarities to Martian landscapes of interest (i.e., Jezero crater—[13]) and the presence of well-documented data and bibliography studies available for comparison with observations made through PRISMA.

Table 1. Geographic position of the two PRISMA products analyzed for the two terrestrial sites selected.

Area	Latitude Range [Deg]	Longitude Range [Deg]	PRISMA Product Name
Gobi Lake	44.974–45.302	100.442–100.911	PRS_L2D_STD_20210629041841_20210629041845_0001
Dalinouer	43.999–44.327	113.485–113.951	PRS_L2D_STD_20230829032232_20230829032236_0001

The Gobi Valley (Figure 1a), located in Mongolia, has undergone geological and hydrological analysis, particularly around the endorheic basin of Orog Nuur [15]. This region lies within a large tectonic depression that formed during the Carboniferous period and served as a primary sediment accumulation area during extended subsidence periods from the Permian through the Jurassic [16].



(**a**) (**b**)

Figure 1. (**a**) Satellite view of the Gobi Valley in Mongolia, showing the vast tectonic depression located between the Hangay and Gobi Altai mountain ranges. (**b**) Detail of the Gobi Valley with specification of the areas of interest (ROI). ROI1 and ROI2 are located near Lake Orog, while ROI3 is located near Lake Böön Tsagaan. "ROI 1: 45°0.424′N 100°44.235′E", "ROI 2: 45°2.668′N 100°45.967′E" and "ROI 3: 45°26.781′N 99°59.717′E", (QGIS source).

The main river of the valley, the Tuin River, stretching about 250 km, has shaped the local geomorphology through the creation of extensive alluvial plains and river terraces, which have undergone various phases of abandonment and reactivation, as described by several authors including [17–19].

In the Gobi Valley region, we have identified and selected three specific areas of interest for our study, centered at 45°17.556′N 100°18.341′E (Figure 1b), and focused around two significant lacustrine sites: two areas near Orog Lake (ROI1 and ROI2), and a third near Böön Tsagaan Lake (ROI3).

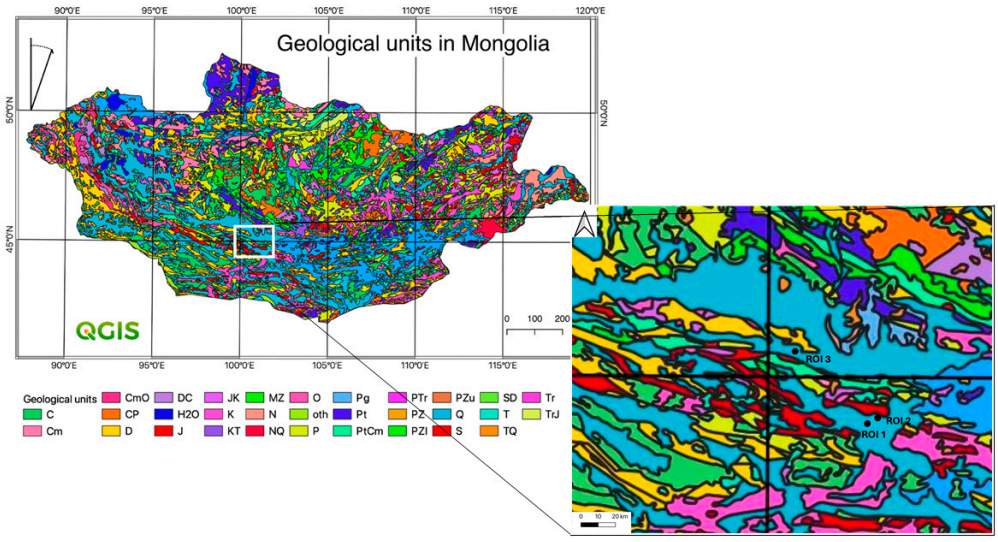
Orog Nuur, the main lacustrine basin in the valley, has been the subject of numerous studies examining the sedimentary input from the alluvial fans of the Gurvan Bogd mountain range to the south and from the Tuin River deposits to the north. These sediments have played a crucial role in shaping the current profile of the lake, which has been significantly influenced by aridification that began in the Cenozoic due to the uplift of the Hangay and Altai mountain ranges. This phenomenon has led to the preservation of alluvial fan surfaces from the Pleistocene to the present day, providing a unique window into the geological evolution of the region [20].

This region, according to some in situ analyses (e.g., [21]), presents a rich geological diversity, hosting a wide range of rocks including granitoids, characterized by their light color and granular composition, and mafic and intermediate rocks, darker and rich in pyroxene and olivine, as well as various types of sediments. These sediments, formed through deposition processes over extended geological periods, add another layer of complexity to the landscape, offering a comprehensive overview of the environmental dynamics and geological processes that shaped the area over time. The presence of such a variety of rocks and sediments makes the Gobi Lakes area a site of particular interest for geological studies, providing a unique opportunity to examine the interactions between different geological processes and their manifestations in the landscape.

Field analyses [22], characterizing the ROIs under study, highlight the presence of minerals typical of a rich sedimentary environment (i.e., calcite, quartz, albite, illite, chlorite).

It would be, thus, possible to perform a direct comparison with spectra acquired from orbit by PRISMA, thus laying the foundations for a more in-depth understanding of the geological and mineralogical processes that characterize these areas.

In the global geological map created by [19], the areas of interest (ROI 1, ROI 2, and ROI 3) have been identified as part of the Quaternary zone (Figure 2). This area is characterized by the presence of basalts and loose sediments such as clay, sand, and gravel. The composition of the substrate indicates recent geological processes that have contributed to the formation of these sediments through erosion and deposition processes. The presence of basalts, in particular, suggests past volcanic activity that has had a significant impact on the surface geology of the region [23].



(**a**) (**b**)

Figure 2. (**a**) Geologic units of Mongolia. Data: USGS geological survey [19]. The white box indicates the area containing the three ROIs. (**b**) Location of the three analyzed ROIs. The three areas of interest are situated within the Quaternary basalt fields (Q) of the blue unit, which form gently undulating surfaces.

Even if this area is not fully compatible with the environment of Jezero crater delta found on Mars, the possibility of comparing remote-sensing data with on-field analysis allows us to verify the accuracy of our spectral data and refine the analysis techniques, laying the foundations for a more in-depth understanding of the geological and mineralogical processes that characterize these areas. The synergy between spectral data and in situ analyses is fundamental to validate our hypotheses and to extend our knowledge of the similarities and differences between terrestrial and Martian landscapes.

On the contrary, to perform a complete comparative analysis between delta formations on Earth and those on Mars, it has been essential to explore other environments characterized by a prevalence of basaltic rocks. This choice was driven by the need to find terrestrial areas morphologically and mineralogically similar to the Martian deltas. Basalt, in fact, constitutes one of the most widespread mineralogical components on Mars, playing a key role in the composition of its soil and rock formations. We, therefore, shifted our attention to the Dalinouer area (North-East China) (Figure 3) and, in particular, on a specific paleo-delta therein, located at 44°N 113°E, showing intense basalt activity similar to that of the present delta in the Martian Jezero crater. This choice has been driven by the study by [24] that pointed out the importance of basaltic formations in the sedimentation mechanisms of deltas, offering an interesting perspective on the possible connections between terrestrial sedimentary dynamics and the Martian ones.

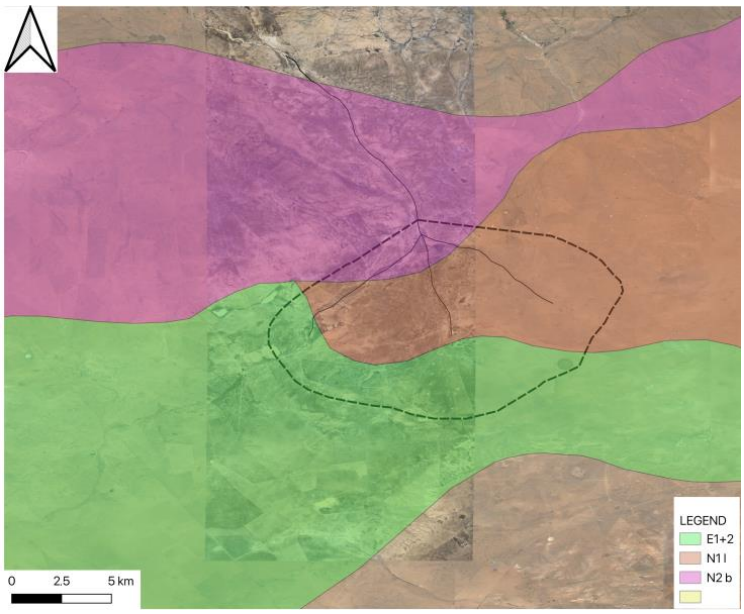


Figure 3. Caption for the extracted geological map of the Dalinouer delta area, originally published at a scale of 1:1,500,000 by the Geological Publishing House. N1 l = Formation Laoliangdi Fm Greyish yellow, dark grey clastics (Mesozoic-Cenozoic); E1 + 2 = Sedimentary Rock (Tertiary-Palaeogene).

During the Cretaceous, the region witnessed the formation of rifted basins, alkaline granitoid plutons, and metamorphic core complexes, likely associated with the subduction of the Pacific Plate beneath Eastern China. In the Cenozoic era, extensive volcanism in the Xilingol area and the adjacent regions of Inner Mongolia and Dariganga in southeastern Mongolia led to the development of extensive volcanic rock units, along with Mesozoic intermediate-acidic intrusions such as diorite and quartz diorite. However, the origin of these magmas remains unclear. The geological layers in the area mainly consist of the Pliocene Baogedawula Formation, the Pleistocene Abaga Formation, and Quaternary sediments, with a limited presence of Paleozoic and Mesozoic layers [25,26].

The Abaga–Dalinuoer volcanic field, together with the Dariganga volcanic field in Mongolia, forms one of the largest basaltic lava plateaus in East Asia, the emplacement of which began in the Middle Miocene and continued until the Pleistocene. This field is characterized by at least 100 volcanic cones distributed along several NEE-oriented faults and covers an area of about 10,000 km^2. This intense Cenozoic volcanic activity is indicative of predominantly alkaline continental intraplate volcanism, with a minor presence of tholeiitic series. The increasing geochemical and geodynamic understanding of this region helps to unravel the mechanisms responsible for intraplate volcanism, which are not fully explained by traditional plate tectonics [25,26].

In the context of studying the geological map of the Nei Mongol Autonomous Region of the People's Republic of China, published at a scale of 1:1,500,000 by the Geological Publishing House and compiled by the Bureau of Geology and Mineral Resources of the Nei Mongol Autonomous Region [27], a detailed picture of the geological composition of the delta under examination emerges. This area is distinctly characterized by the presence of sedimentary rocks (Figure 3). Specifically, clasts of yellow-brown and brick-red color, which contain calcareous concretions (N2 b, N1 l, E1 + 2), are observed. These sediments are deposited over the underlying magmatic rocks, covering them and, thus, influencing the morphology and chemical-physical composition of the delta.

The comparison of this area with the delta in Jezero crater primarily stems from the morphology and sediment deposition. Both deltas (Dalinouer and Jezero) are now dry and exhibit typical features of river deltas, including lobate structures and the presence

of channels that fork and rejoin, forming a complex network that indicates a history rich in fluvial events. Studying this terrestrial paleo-delta provides researchers with valuable data to better understand how deltas form and evolve in arid and semi-arid environments, both on Earth and on Mars. This can help to better interpret the geological processes of the Martian past, offering insights into the past presence of water and the environmental conditions that might eventually have been conducive to life.

2.4. PRISMA Data Reduction

In order to correctly and easily manage the PRISMA cubes selected for analysis, we developed a Python software (v 1.0) provided with a GUI (graphical user interface), named ssdcPRISMAreader.py, allowing a series of operations on the cube.

The first of them is the possibility of displaying a quick look of the PRISMA field of view in RGB colors, using three standard bands mimicking the human vision.

Once this visualization has been made, the user can choose different options, from inspecting and save spectra belonging to single PRISMA pixels to the possibility of zooming in a specific area and then selecting a rectangular area over which all the spectra are averaged and saved in tabular form, with ancillary information, such as number of pixels over latitude and longitude, latitude and longitude limits, and standard deviation of the mean spectrum saved.

Apart from these capabilities, maybe the most useful one implemented in ssdcPRISMAreader.py is that allowing the photometric correction of PRISMA spectra. This operation is well-known to enable accurate comparison of spectra acquired under different illumination conditions, due to the solar illumination angle, terrain topography, or spacecraft position.

Similarly to the CRISM data here used, PRISMA L2D already underwent an atmospheric correction algorithm, but, differently to the CRISM ones, PRISMA data released by the system are not photometrically corrected. In order to make it possible to compare the two datasets, this operation over PRISMA data is, thus, required.

The most-used photometric techniques can be considered the Lambert and Lommel-Seeliger ones, where the main difference among them is that the former only considers correction using the incidence angle, taking a fixed emergence angle of 30°, whereas the latter allows to accurately define the incidence and emission angles coming from real observation conditions.

We implemented both of them in ssdcPRISMAreader.py, so that the user can chose what technique to use. However, the main effort in making this correction available was to provide every PRISMA cube of interest of a detailed digital elevation model (DEM), used as input to compute emergence and incidence angles. Original PRISMA data are natively provided with emergence and incidence angles for every pixel only relative to the standard Earth ellipsoid and, therefore, these data cannot be used for a detailed and useful photometric correction.

We used 30 m/px ASTER DEMs (https://cmr.earthdata.nasa.gov/search/concepts/C1220567908-USGS_LTA.html—accessed on 19 February 2025), by means of which we were able to compute the slope and aspect for every pixel of the scene.

This input was not the only thing needed for the computation, since, in order to correctly compute the needed angles, the exact position in space of Earth, then Sun, and spacecraft in the exact moment of the observation is required.

In order to do so, we started from the method described by [28], making it possible to use only astronomical parameters to computer vectors from the Sun to the Earth, and expanding this approach to compute also vectors from S/C to the Earth.

In particular, naming observer's coordinates (latitude and longitude) as (φ0, λ0) and subsolar point's coordinates (φs, λs), [24] found that the x-, y-, and z-components of the unit vector S pointing from the observer to the center of the Sun are defined as follows:

$$Sx = \cos \varphi s \sin (\lambda s - \lambda 0)$$

$$Sy = \cos \varphi 0 \sin \varphi s - \sin \varphi 0 \cos \varphi s \cos (\lambda s - \lambda 0)$$

$$Sz = \sin \varphi 0 \sin \varphi s - \cos \varphi 0 \cos \varphi s \cos (\lambda s - \lambda 0)$$

By using the S/C coordinates instead of solar ones, we expanded this approach also to compute the unit vector pointing from the observer to the center of the S/C.

Thanks to this method, in our work, it has been possible to use photometric-corrected PRISMA spectra, so that a robust comparison with Martian CRISM spectra has been possible.

Finally, on the photometrically corrected PRISMA data, with the aim of enhancing the spectral features of minerals, we used the ratio between the target spectra and the average spectrum of all the images, excluding only the pixels related to the water bodies and clouds.

3. Results

3.1. Gobi Lakes

Mineralogical on field analyses of sediments in ROI 1, 2, 3 [22] revealed the presence of quartz, albite, illite, smectite, chlorite, and calcite.

The PRISMA data analyzed and corresponding to the ROIs investigated by [18] allowed to identify all minerals present in the scenes [14] (Figure 4).

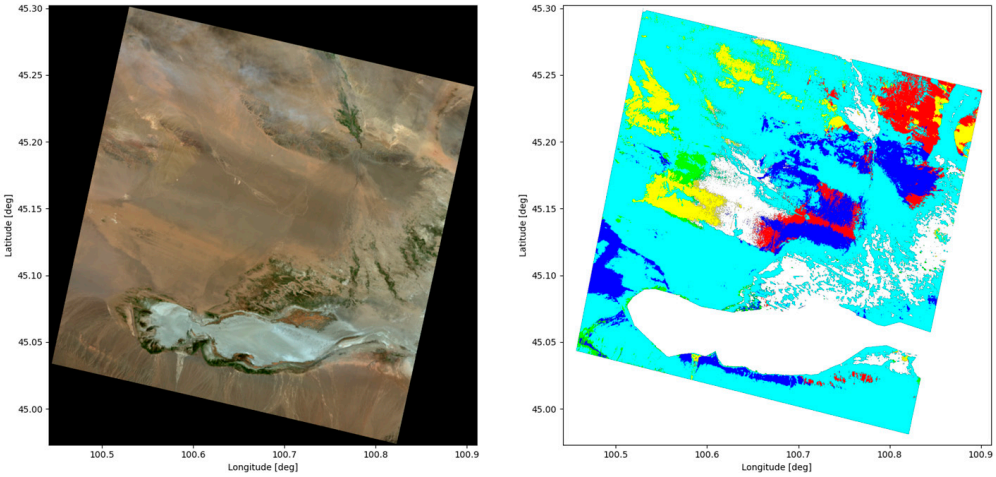


Figure 4. Left: RGB (red = 645.9 nm, green = 550.9, blue = 475.3 nm) visualization of the PRISMA acquisition over the Gobi Lake area studied here. **Right**: Map of the mineral distribution on the same area, using PRISMA hyperspectral data: Cyan is for quartz (the full spectral range), blue for chlorite (absorptions at 2.25 and 2.33 μm), yellow for albite (all the spectral range), green for montmorillonite, and red for illite (these latter at 2.19 and 2.20 μm, distinguished by the absorption width). PRISMA Product—©ASI—Agenzia Spaziale Italiana—(2020). All rights reserved.

In particular, as reported by [29], illite was identified on the basis of the main absorption near 2.20 μm and a weak one around 2.35 μm. This last absorption allowed to distinguish between illite and smectite. Chlorite was identified on the basis of the co-presence of absorptions at 2.25–2.33 μm, whereas calcite was identified by a broad absorption around 2.34 μm. Since quartz and albite are featureless in the range of PRISMA, they were identified by comparison of the profile shape with albite and quartz from the USGS spectral library [30].

The presence of quartz and albite in the sediments of ROI 3 is generally spatially correlated with the occurrence of granitoids in the region [21].

As a consequence, smectite (montmorillonite) and illite are interpreted as secondary minerals formed by the alteration of feldspars, whereas the presence of chlorite can be assigned either to the alteration of femic minerals, biotite or amphiboles (hornblende) in granitoids, or to the weathering of olivine, pyroxenes, and hornblende in basalts, also present in this complex region. The presence of calcite has to be assigned to groundwater activities.

3.2. Dalinouer Area

The Dalinouer area is characterized by basaltic rocks: basanites, tholeiitic basalts, peridotites, and pyroxenites [25]. Therefore, the delta firstly individuated by [24] (Figure 5) could potentially include femic minerals (e.g., pyroxenes, olivines, carbonates), similarly to what we observe in Martian deltas.

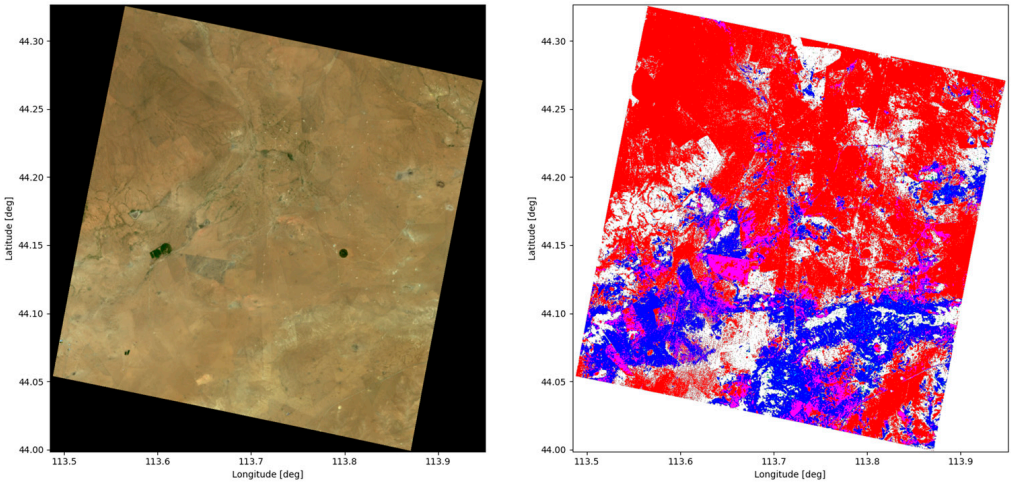


Figure 5. Left: RGB (red = 645.9 nm, green = 550.9, blue = 475.3 nm) visualization of the PRISMA acquisition over the Dalinouer area studied here. **Right**: Map of the mineral distribution on the same area, using PRISMA hyperspectral data: Red is for illite/montmorillonite (absorptions at 2.20 μm), blue for femic minerals (olivine/pyroxenes) (absorptions at 1 μm), and magenta for a combination of them. PRISMA Product—©ASI—Agenzia Spaziale Italiana—(2023). All rights reserved.

Differently from the case of the Gobi Lakes site, we could not find literature data on specific mineralogical studies related to sediments in the delta of Dalinouer area, but we can use the ground-orbit matching found for the Gobi Lakes site to perform a detailed mineralogical analysis using only PRISMA data.

From the geological study of Abaga-Dalinouer volcanic field [16] and the geological map of Inner Mongolia [27], we know that the Dalinouer site chosen (Figure 6) is located in the nearby of the volcanic area of Abaga-Dalinouer.

This area is characterized by basalts (unit β3 of the geological map, Miocene to Pleistocene [31]), but it also comprises granitoid units (unit γ2 of the geological map, Middle-to-Late Jurassic geological map [27]) and clastic rocks consisting of marlstones, basalts, and Ca-sulfates (units E1-2 and N1–N2 of the geological map, Paleo to Neogene [27]) (Figure 5).

It is, therefore, reasonable to expect the delta sediments to have a very complex mineralogical composition.

The PRISMA data on this area revealed an overall dominant presence of spectral signatures featureless in the VIS/NIR spectral range (i.e., 0.48–2.4 μm), compatible with quartz/silica microcrystalline and albite (Figure 7) for the presence of granitoids in this area.

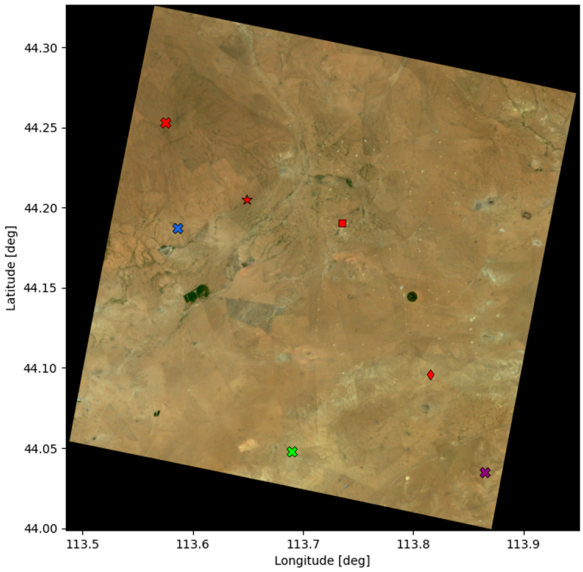


Figure 6. RGB visualization of the PRISMA acquisition over the Dalinouer site studied, with overimposed symbols showing the pixels where spectra in Figures 7–10 have been acquired. PRISMA Product—©ASI—Agenzia Spaziale Italiana—(2023). All rights reserved.

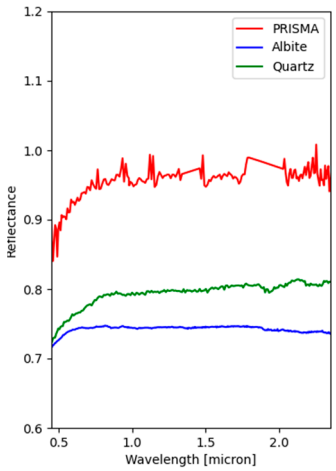


Figure 7. Comparison between a PRISMA spectrum, acquired at the red star symbol in Figure 6, and laboratory spectra of albite and quartz.

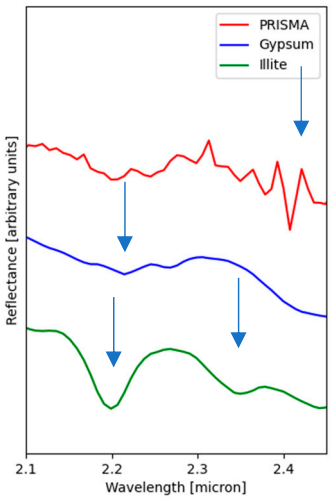


Figure 8. Comparison between a PRISMA spectrum, acquired at the red diamond symbol in Figure 6, and laboratory USGS [30] spectra of gypsum (HS333.3B) and illite (IL101 2M2). Arrows indicate the diagnostic absorption of gypsum and illite in NIR.

Spectral absorptions were also found around 2.19–2.21 μm (Figure 8) and near 2.44. These features can be attributed to clay minerals and to Ca sulphates like gypsum.

Both these minerals occur in the area of the delta.

Some other signatures are characterized by absorptions around 1 and 2 μm, typical of Ca bearing pyroxenes and olivine (Figure 9), thus showing the presence of basaltic rocks.

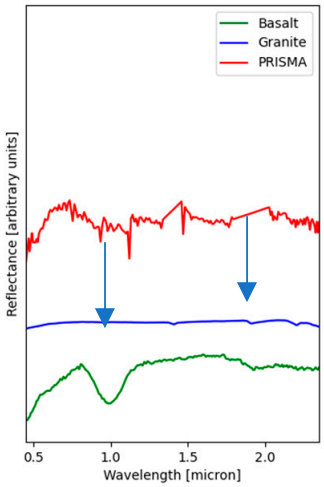


Figure 9. Comparison between a PRISMA spectrum, acquired at the red square symbol in Figure 6, and USGS [30] laboratory spectra of basalt (Mafic Basalt.H1) and pigeonite (HS199.3B). Arrows indicate the absorption features of reference basalt in this range. The diagnostic absorption features at 1 μm and near to 2 μm are due to pyroxene and olivine femic minerals.

Furthermore, with respect to these minerals that confirmed the rock varieties in this area, other spectral signatures in the 2–2.5 μm spectral range were interpreted as alterations of femic minerals: Mg, Fe-clays such as minerals from chlorite and serpentine groups and the possible hydrothermal alteration of feldspar (buddingtonite) (Figure 10).

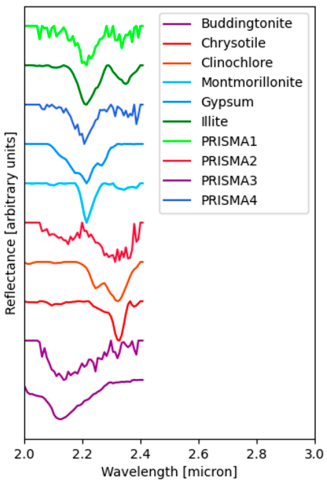


Figure 10. Comparison between PRISMA spectra acquired at the X symbol of the corresponding color in Figure 6, and USGS [30] laboratory spectra of buddingtonite (NHB2301), chrysotile (HS323.1B), clinochlore (NMNH83369), montmorillonite (SCa-2), and gypsum (SU2202). The 2-2.5 μm range is used to better show diagnostic absorption bands of the minerals of interest.

4. Discussion

The CRISM data in Jezero crater showed the dominant presence of olivine and Ca-Fe-Mg carbonates spectra, with alteration minerals such as Mg-Fe smectites [32–34].

In the case of Jezero delta, the olivine represented the basement in which, after an impact, the formation of carbonates from the interaction with base olivine and CO_2 started.

The interaction of groundwater and rocks in and around the crater caused the formation of Mg-Fe smectites.

In our study, we had two terrestrial water-related environments to compare: one dominated by acidic rocks, in the Gobi Lakes area, and another, presently dry, by basaltic rocks in the volcanic field of Dalinouer area.

The first site in Gobi Lake area showed a mineralogy resulting from the occurrence of granites, sand-quartz- and albite-based, plus secondary minerals like illite, smectite, and chlorite. Moreover, the presence of carbonates formed by groundwaters can be studied as analogs for the carbonates formed by groundwaters in Jezero crater.

The paleo-delta located in the Dalinouer site is predominantly covered by illite/montmorrillonite, although femic features appear in localized small areas, which can be due to exposed boulders and outcrops (Figure 5). In fact, femic features become dominant in the area of mountains, where the sand does not settle.

As reported by [35], the delta in Jezero appears to be formed by sediments containing femic minerals (Figure 3 by [35]).

In summary, in the paleo-delta in Abaga-Dalinouer area, we found (even if with weaker features with respect to Jezero) clear olivine-pyroxene spectral features, Ca-sulphates, and carbonates (Figure 11), and, as clay minerals, we found evidence of the hydrous alteration of femic minerals, like ones from serpentine groups (Figure 12).

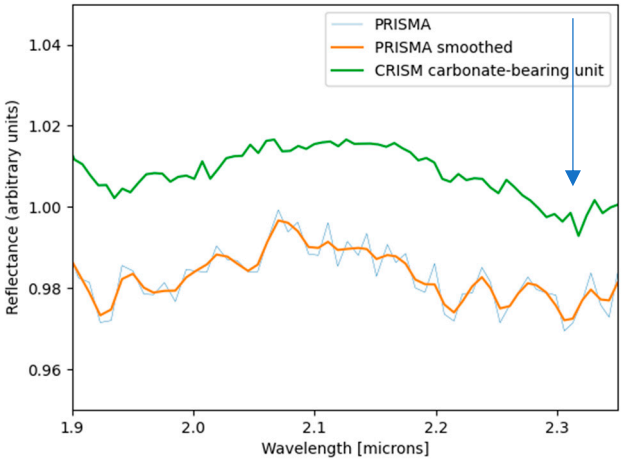


Figure 11. Comparison between a PRISMA spectrum (smoothed), same as the "PRISMA 2" spectrum in Figure 10, and a CRISM carbonate-bearing unit Jezero crater, as reported by [35]. The arrow highlights diagnostic absorption feature of carbonates.

The difference in the main mineralogy between the terrestrial hydrological environments investigated in this work and the delta in Jezero crater is related to different geological and environmental factors, and also the water/rock ratio, and water pH differences could influence the weathering products and differences in the Earth–Mars relation. The scarcity of silicic rocks (such as granites, in which quartz occurs) on Mars is related to the planet's water activity and the absence of plate tectonics, which are crucial for producing silica-rich magmas. On the other hand, on Earth, vegetation and erosion make difficult the preservation of femic minerals, such as olivine.

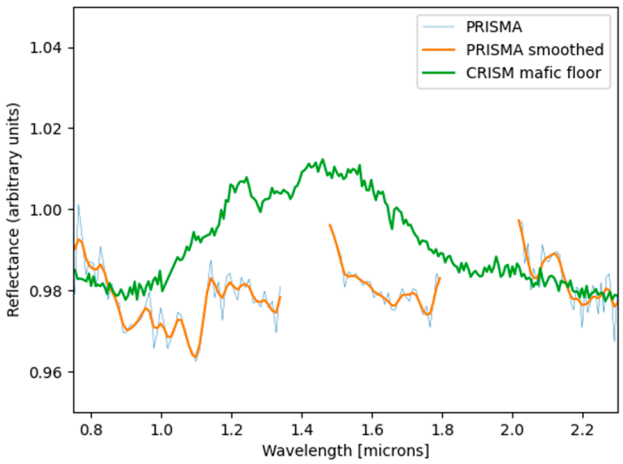


Figure 12. Comparison between a PRISMA spectrum (smoothed), acquired at the red square symbol in Figure 6, and a CRISM spectrum representing mafic floor at Jezero crater, as reported by [35].

However, the paleo-delta in the Dalinouer area is an interesting site that can be studied as an analogue of Jezero, due to the presence of subsisting femic spectral features clearly indicating the occurrence of basaltic rocks. In this area, we also identified evidence of carbonate absorptions (Figure 11), Ca-sulphates (Figure 8), and, for the first time, we remotely found evidence of the hydrous alteration of femic minerals, like ones from serpentine groups (Figure 10). Carbonates, Ca- sulphates, and serpentine group minerals were also found in the Jezero crater on Mars [36,37].

5. Conclusions

The main aim of the study here presented was to demonstrate the feasibility of the usage of the terrestrial ASI PRISMA hyperspectral data as a kind of "missing link" between Earth ground-truth studies and Martian remote-sensing observations over areas with on the two planets with similar geological histories.

We therefore looked for an arid zone on Earth for which previous on-field literature works had identified specific mineralogical components, succeeding in identifying them also from the orbital point of view of PRISMA.

For the Gobi Lake areas here specifically analyzed, we found a granitic-based environment, with the spread presence of quartz and albite and illite, with smectite and chlorite as secondary phases, thus confirming the results expected by on-field analysis.

This result allowed us to finally proceed to really compare an area on Earth and one on Mars with similar known geological evolutions, always keeping in mind the intrinsic differences between the two planetary environments, but with the possibility of linking what was found by remote-sensing instruments with what was really to be expected on the ground for both planets.

In order to do that, we selected the paleo-deltas in the Dalinouer region on Earth and in the Jezero crater on Mars, primarily because of their similar geomorphological features.

Even if there are differences in the instrumentations used for Earth and Mars, for example, PRISMA has a restricted spectral range with respect to CRISM, thanks to the adoption of advanced spectral comparison techniques (e.g., the ratio between target spectrum and average featureless spectrum allowing the enhancement of the spectral features really occurring), the conducted spectral analysis finally confirmed the similarity between the two areas, with a mesoscale basaltic mineralogy, and evidence of carbonates from groundwaters. Moreover, we found spectral features of minerals that on Mars have an astrobiological potential, such as silica, serpentine, and gypsum, indicating that the area in the Dalinouer site can be a promising site as a terrestrial analogue even for astrobiological studies.

Apart from the expected intrinsic properties of the two planets, in this work, we therefore demonstrated that PRISMA data can be used to remotely investigate terrestrial analogues of planetary surfaces. This work also allowed to integrate ASI PRISMA data in common planetary-sciences data reduction pipeline software, another step towards the integration of the two branches, with the final goal of including the Earth inside the more general planetary exploration community.

These results suggest the opportunity for a future tighter interaction between two scientific communities, the Earth-observation one and the planetary-geology one, that could result in great advantages from this proposed connection, in order to better understand data acquired from planetary environments different from the Earth, but with evident similarities, thus helping in planning and defining the next steps in Martian exploration.

Author Contributions: Conceptualization, all authors; methodology, all the authors; software, A.Z.; investigation, P.M., A.Z. and V.C.; writing—original draft preparation, A.Z., P.M. and V.C.; writing—review and editing, all authors. All authors have read and agreed to the published version of the manuscript.

Funding: This research received no external funding.

Data Availability Statement: PRISMA data can be retrieved upon registration to the ASI PRISMA portal. CRISM data are publicly available on the PDS Geoscience Node. The ssdcPRISMAreader.py software can be requested by contacting angelo.zinzi@asi.it.

Acknowledgments: V.C. acknowledges financial support from the ASI-INAF agreement n. 2022-14-HH.0.

Conflicts of Interest: The authors declare no conflicts of interest.

References

1. Hand, E. Phoenix descending. *Nature* **2008**, *453*, 142. [CrossRef] [PubMed]
2. Changela, H.G.; Chatzitheodoridis, E.; Antunes, A.; Beaty, D.; Bouw, K.; Bridges, J.C.; Capova, K.A.; Cockell, C.S.; Conley, C.A.; Dadachova, E.; et al. Mars: New insights and unresolved questions. *Int. J. Astrobiol.* **2022**, *21*, 46. [CrossRef]
3. Calvin, W.M.; King, T.V.V.; Clark, R.N. Hydrous carbonates on Mars?: Evidence from Mariner 6/7 infrared spectrometer and ground-based telescopic spectra. *J. Geophys. Res.* **1994**, *99*, 14659–14676. [CrossRef]
4. Erard, S.; Bibring, J.-P.; Mustard, J.; Forni, O.; Head, J.W.; Hurtrez, S.; Langevin, Y.; Pieters, C.M.; Rosenqvist, J.; Sotin, C.; et al. Spatial variations in composition of the Valles Marineris and Isidis Planitia regions of Mars derived from ISM data. In *IN: Lunar and Planetary Science Conference, 21st, Houston, TX, 12–16 March 1990, Proceedings (A91-42332 17-91)*; CNES-Supported Research; Lunar and Planetary Institute: Houston, TX, USA, 1991; pp. 437–455.
5. Murchie, S.; Arvidson, R.; Bedini, P.; Beisser, K.; Bibring, J.; Bishop, J.; Boldt, J.; Cavender, P.; Choo, T.; Clancy, R.T.; et al. Compact reconnaissance imaging spectrometer for Mars (CRISM) on Mars reconnaissance orbiter (MRO). *J. Geophys. Res. Planets* **2007**, *112*, e5. [CrossRef]
6. Domagal-Goldman, S.D.; Wright, K.E.; Adamala, K.; De La Rubia, L.A.; Bond, J.; Dartnell, L.R.; Goldman, A.D.; Lynch, K.; Naud, M.-E.; Paulino-Lima, I.G.; et al. The astrobiology primer v2. 0. *Astrobiology* **2016**, *16*, 561. [CrossRef]
7. Kereszturi, A. Review of Wet Environment Types on Mars with Focus on Duration and Volumetric Issues. *Astrobiology* **2012**, *12*, 586–600. [CrossRef] [PubMed]
8. Caporusso, G.; Lopinto, E.; Lorusso, R.; Rosa, L.; Rocchina, G.; Girolamo, D.M.; Patrizia, S. The Hyperspectral Prisma Mission in Operation. In Proceedings of the IGARSS 2020—2020 IEEE International Geoscience and Remote Sensing Symposium, Waikoloa, HI, USA, 26 September–2 October 2020. [CrossRef]
9. Ovchinnikova, A.; Jaumann, R.; Walter, S.H.; Gross, C.; Zuschneid, W.; Postberg, F. A modeling approach for water and sediment transport in Jezero crater on Mars based on new geomorphological evidence. *Icarus* **2025**, *426*, 116349. [CrossRef]
10. Steinmann, V.; Bahia, R.S.; Kereszturi, A. Selecting Erosion-and Deposition-Dominated Zones in the Jezero Delta Using a Water Flow Model for Targeting Future In Situ Mars Surface Missions. *Remote Sens.* **2024**, *16*, 3649. [CrossRef]
11. Holm-Alwmark, S.; Kinch, K.M.; Hansen, M.D.; Shahrzad, S.; Svennevig, K.; Abbey, W.J.; Anderson, R.B.; Calef, F.J.; Gupta, S.; Hauber, E.; et al. Stratigraphic Relationships in Jezero Crater, Mars: Constraints on the Timing of Fluvial-Lacustrine Activity From Orbital Observations. *J. Geophys. Res.* **2021**, *126*, e2021JE006840. [CrossRef]

12. Goudge, T.A.; Milliken, R.E.; Head, J.W.; Mustard, J.F.; Fassett, C.I. Sedimentological evidence for a deltaic origin of the western fan deposit in Jezero crater, Mars and implications for future exploration. *Earth Planet. Sci. Lett.* **2017**, *458*, 357–365. [CrossRef]
13. Goudge, T.A.; Mustard, J.F.; Head, J.W.; Fassett, C.I.; Wiseman, S.M. Assessing the mineralogy of the watershed and fan deposits of the Jezero crater paleolake system, Mars. *J. Geophys. Res. Planets* **2015**, *120*, 775–808. [CrossRef]
14. Ori, G.G.; Rossi, A.P.; Komatsu, G.; Ormo, J.; Rainone, M.; Signanini, P.; Torrese, P.; Sammartino, P.; Madonna, R.; Baliva, A.; et al. Seismic Data from the Main Crater of the Proposed Sirente Meteorite Crater Field (Central Italy). In Proceedings of the 38th Lunar and Planetary Science Conference, (Lunar and Planetary Science XXXVIII), League City, TX, USA, 12–16 March 2007; p. 1092, LPI Contribution No. 1338.
15. Daxner-Höck, G.; Badamgarav, D. Geological and stratigraphic setting. Annalen des Naturhistorischen Museums in Wien. Serie A für Mineralogie und Petrographie, Geologie und Paläontologie, Anthropologie und Prähistorie. 2006, pp. 1–24. Available online: https://www.jstor.org/stable/41702093 (accessed on 19 February 2025).
16. Erdenetsogt, B.O.; Lee, I.; Bat-Erdene, D.; Jargal, L. Mongolian coal-bearing basins: Geological settings, coal characteristics, distribution, and resources. *Int. J. Coal Geol.* **2009**, *80*, 87–104. [CrossRef]
17. Walther, M. Paläoklimatische Untersuchungen zur jungpleistozänen Landschaftsentwicklung im Changai-Bergland und in der nördlichen Gobi. *Petermanns Geogr. Mitteilungen* **1998**, *142*, 207–217.
18. Lehmkuhl, F.; Lang, A. Geomorphological investigations and luminescence dating in the southern part of the Khangay and the Valley of the Gobi Lakes (Central Mongolia). *J. Quat. Sci. Publ. Quat. Res. Assoc.* **2011**, *16*, 69–87. [CrossRef]
19. Lehmkuhl, F.; Nottebaum, V.; Hülle, D. Aspects of late Quaternary geomorphological development in the Khangai Mountains and the Gobi Altai Mountains (Mongolia). *Geomorphology* **2017**, *312*, 24–39. [CrossRef]
20. Van der Wal, J.L.; Nottebaum, V.C.; Stauch, G.; Binnie, S.A.; Batkhishig, O.; Lehmkuhl, F.; Reicherter, K. Geomorphological evidence of active faulting in low seismicity regions—Examples from the valley of Gobi lakes, southern Mongolia. *Front. Earth Sci.* **2021**, *8*, 589814. [CrossRef]
21. Guy, A.; Schulmann, K.; Munschy, M.; Miehe, J.; Edel, J.; Lexa, O.; Fairhead, D. Geophysical constraints for terrane boundaries in southern Mongolia. *J. Geophys. Res. Solid Earth* **2014**, *119*, 7966–7991. [CrossRef]
22. Sekine, Y.; Kitajima, T.; Fukushi, K.; Gankhurel, B.; Tsetsgee, S.; Davaasuren, D.; Matsumiya, H.; Chida, T.; Nakamura, M.; Hasebe, N. Hydrogeochemical Study on Closed-Basin Lakes in Cold and Semi-Arid Climates of the Valley of the Gobi Lakes, Mongolia: Implications for Hydrology and Water Chemistry of Paleolakes on Mars. *Minerals* **2020**, *10*, 792. [CrossRef]
23. Lemenkova, P. Gobi Altai, Khangai and Khentii Mountains mapped by a mixed-method cartographic approach for comparative geophysical analysis. *Mong. Geosci.* **2021**, *26*, 62–79. [CrossRef]
24. Scuderi, L.A.; Mason, D.P. Gobi Desert Deltas as Analogs for Jezero Delta Mars. In Proceedings of the Workshop on Terrestrial Analogs for Planetary Exploration, Online, 16–18 June 2021; LPI Contribution No. 2595, id.8083.
25. Zhang, M.; Guo, Z. Origin of Late Cenozoic Abaga–Dalinuoer basalts, eastern China: Implications for a mixed pyroxenite–peridotite source related with deep subduction of the Pacific slab. *Gondwana Res.* **2016**, *37*, 130–151. [CrossRef]
26. Chen, S.S.; Fan, Q.C.; Zou, H.B.; Zhao, Y.-W.; Shi, R.-D. Geochemical and Sr–Nd isotopic constraints on the petrogenesis of late Cenozoic basalts from the Abaga area, Inner Mongolia, eastern China. *J. Volcanol. Geotherm. Res.* **2015**, *305*, 30–44. [CrossRef]
27. Geology of Nei Mongol (Inner Mongolia), Northeastern China [1:1,500,000]. Available online: https://www.orrbodies.com/resource/geology-nei-mongol-inner-mongolia-north-eastern-china/ (accessed on 19 February 2025).
28. Zhang, T.; Stackhouse, P.W., Jr.; Macpherson, B.; Mikovitz, J.C. A solar azimuth formula that renders circumstantial treatment unnecessary without compromising mathematical rigor: Mathematical setup, application and extension of a formula based on the subsolar point and atan2 function. *Renew. Energy* **2021**, *172*, 1333–1340. [CrossRef]
29. Manzari, P.; Camplone, V.; Zinzi, A.; Zinzi, A.; Ammannito, E.; Sindoni, G.; Zucca, F.; Polenta, G. Exploiting Prisma Hypespectral Data to Support CRISM Measurements on Paleo-Hydrological Environments on Mars. In Proceedings of the 13th Workshop on Hyperspectral Image and Signal Processing: Evolution in Remote Sensing, WHISPERS, Athens, Greece, 31 October–2 November 2023.
30. Kokaly, R.F.; Clark, R.N.; Swayze, G.A.; Livo, K.E.; Hoefen, T.M.; Pearson, N.C.; Wise, R.A.; Benzel, W.M.; Low, H.A.; Driscoll, R.L.; et al. *Data: U.S. Geological Survey Data Release*; Version 7; USGS Spectral Library, 2017. Available online: https://www.sciencebase.gov/catalog/item/5807a2a2e4b0841e59e3a18d (accessed on 19 February 2025).
31. Geological Map of Inner Mongolia Autonomous Region, China. Available online: https://ikcest-drr.data.ac.cn/map/m02c7 (accessed on 19 February 2025).
32. Brown, A.J.; Viviano, C.E.; Goudge, T.A. Olivine-Carbonate Mineralogy of the Jezero Crater Region. *J. Geophys. Res. Planets* **2020**, *125*, e2019JE006011. [CrossRef]
33. Ehlmann, B.L.; Mustard, J.F.; Fassett, C.I.; Schon, S.C.; Iii, J.W.H.; Marais, D.J.D.; Grant, J.A.; Murchie, S.L. Clay minerals in delta deposits and organic preservation potential on Mars. *Nat. Geosci.* **2008**, *1*, 355–358. [CrossRef]
34. Ehlmann, B.L.; Mustard, J.F.; Murchie, S.L.; Poulet, F.; Bishop, J.L.; Brown, A.J.; Calvin, W.M.; Clark, R.N.; Marais, D.J.D.; Milliken, R.E.; et al. Orbital Identification of Carbonate-Bearing Rocks on Mars. *Science* **2008**, *322*, 1828–1832. [CrossRef] [PubMed]

35. Horgan, B.H.N.; Anderson, R.B.; Dromart, G.; Amador, E.S.; Rice, M.S. The mineral diversity of Jezero crater: Evidence for possible lacustrine carbonates on Mars. *Icarus* **2020**, *339*, 113526. [CrossRef]
36. Phua, Y.Y.; Ehlmann, B.L.; Siljestrom, S.; Czaja, A.D.; Beck, P.; Connell, S.; Wiens, R.C.; Jakubek, R.S.; Williams, R.M.E.; Zorzano, M.; et al. Characterizing Hydrated Sulfates and Altered Phases in Jezero Crater Fan and Floor Geologic Units with SHERLOC on Mars 2020. *J. Geophys. Res. Planets* **2024**, *129*, e2023JE008251. [CrossRef]
37. Bosak, T.; Shuster, D.L.; Scheller, E.L.; Siljeström, S.; Zawaski, M.J.; Mandon, L.; Simon, J.I.; Weiss, B.P.; Stack, K.M.; Mansbach, E.N.; et al. Astrobiological Potential of Rocks Acquired by the Perseverance Rover at a Sedimentary Fan Front in Jezero Crater, Mars. *AGU Adv.* **2024**, *5*, e2024AV001241. [CrossRef]

Disclaimer/Publisher's Note: The statements, opinions and data contained in all publications are solely those of the individual author(s) and contributor(s) and not of MDPI and/or the editor(s). MDPI and/or the editor(s) disclaim responsibility for any injury to people or property resulting from any ideas, methods, instructions or products referred to in the content.